Radiometric correction of multi-temporal Landsat data for characterization of early successional forest patterns in western Oregon

Todd A. Schroeder [a,*], Warren B. Cohen [b], Conghe Song [c], Morton J. Canty [d], Zhiqiang Yang [a]

[a] Department of Forest Science, Oregon State University, Corvallis, OR 97331, United States
[b] Forestry Sciences Laboratory, Pacific Northwest Research Station, USDA Forest Service, 3200 SW Jefferson Way, Corvallis, OR 97331, United States
[c] Department of Geography, University of North Carolina, Chapel Hill, NC, 27599, United States
[d] Systems Analysis and Technology Evaluation, Jülich Research Center, D-52425 Jülich, Germany

Abstract

Detecting and characterizing continuous changes in early forest succession using multi-temporal satellite imagery requires atmospheric correction procedures that are both operationally reliable, and that result in comparable units (e.g., surface reflectance). This paper presents a comparison of five atmospheric correction methods (2 relative, 3 absolute) used to correct a nearly continuous 20-year Landsat TM/ETM+ image data set (19-images) covering western Oregon (path/row 46/29). In theory, full absolute correction of individual images in a time-series should effectively minimize atmospheric effects resulting in a series of images that appears more similar in spectral response than the same set of uncorrected images. Contradicting this theory, evidence is presented that demonstrates how absolute correction methods such as Second Simulation of the Satellite Signal in the Solar Spectrum (6 s), Modified Dense Dark Vegetation (MDDV), and Dark Object Subtraction (DOS) actually make images in a time-series somewhat less spectrally similar to one another. Since the development of meaningful spectral reflectance trajectories is more dependant on consistent measurement of surface reflectance rather than on accurate estimation of true surface reflectance, correction using image pairs is also tested. The relative methods tested are variants of an approach referred to as "absolute-normalization", which matches images in a time-series to an atmospherically corrected reference image using pseudo-invariant features and reduced major axis (RMA) regression. An advantage of "absolute-normalization" is that all images in the time-series are converted to units of surface reflectance while simultaneously being corrected for atmospheric effects. Of the two relative correction methods used for "absolute-normalization", the first employed an automated ordination algorithm called multivariate alteration detection (MAD) to statistically locate pseudo-invariant pixels between each subject and reference image, while the second used analyst selected pseudo-invariant features (PIF) common to the entire image set. Overall, relative correction employed in the "absolute-normalization" context produced the most consistent temporal reflectance response, with the automated MAD algorithm performing equally as well as the handpicked PIFs. Although both relative methods performed nearly equally in terms of observed errors, several reasons emerged for preferring the MAD algorithm. The paper concludes by demonstrating how "absolute-normalization" improves (i.e., reduces scatter in) spectral reflectance trajectory models used for characterizing patterns of early forest succession.
© 2006 Elsevier Inc. All rights reserved.

Keywords: Atmospheric correction; Relative normalization; Multivariate alteration detection (MAD); Landsat time-series; Forest succession

1. Introduction

Landsat has been providing a nearly continuous record of global land surface change since 1972. This record represents one of the most consistent available archives of recent earth history information, and its use has facilitated understanding of earth surface processes across spatial and temporal scales and disciplines (Cohen & Goward, 2004).

In forestry, Landsat imagery has been important in characterizing and mapping frequency and extent of forest fire (Miller & Yool, 2002; van Wagtendonk et al., 2004), stand-replacing disturbance (Cohen et al., 1998; Cohen et al., 2002; Sader et al., 2003), partial harvest (Franklin et al., 2000; Healey et al., 2006; Nilson et al., 2001), successional stage (Hall et al., 1991; Mausel et al., 1993) and vegetation regrowth (Foody et al., 1996; Sabol

* Corresponding author. Tel.: +1 541 758 7758.
  E-mail address: todd.schroeder@oregonstate.edu (T.A. Schroeder).

et al., 2002; Viedma et al., 1997). Studies focusing on the highly dynamic process of forest succession have generally relied on forest age class information extracted from single image dates to make inferences about successional stage attributes (Fiorella & Ripple, 1993; Jakubauskas, 1996; Peterson & Nilson, 1993). The difficulty with this approach is that the relationship between forest age and spectral data can be highly variable, especially for young (<20-year) stands with sparse canopy cover (Horler & Ahern, 1986). The reasons for this variability are many, but can include differences in site quality and location, site preparation, planting practices (density and spacing), and species composition. Perhaps even more important is that forest age is not directly remotely sensible in any given date of imagery, as are forest structure and composition, both of which are physically related to forest succession (Cohen et al., 1995).

An alternative use of Landsat for characterizing forest succession is examination of a multi-temporal image series. For any forest stand that has been disturbed since 1972 one could theoretically observe its recovery trajectory, and therefore know both its age and how its structural and compositional attributes have changed over time. However, as described by Song and Woodcock (2003), factors such as seasonal phenology, ground conditions, and atmospheric conditions can contribute to variability in multi-temporal spectral responses that may have little to do with forest succession. In any multi-temporal analysis where the spectral signal is not sufficiently strong to minimize the effects of these complicating factors, radiometric correction is essential to differentiate real change from noise. With adequate correction it may be possible to examine temporal trajectories of Landsat data for a more dynamic characterization of forest succession.

The objective of this paper is to compare the effectiveness of absolute and relative radiometric correction procedures with the ultimate goal of producing consistent temporal reflectance trajectories of forests that are recovering from stand-replacing disturbance. In the strict sense, full absolute image correction involves both application of absolute calibration coefficients for sensor and related parameters and atmospheric correction to derive estimates of surface reflectance. In this study, however, we are also interested in examining results of the intermediate step in which calibration parameters are applied, but atmospheric effects are not removed (i.e., at-satellite reflectance). For clarity, we refer to this as the partially corrected case with absolute calibration only. On the other hand, relative calibration (commonly referred to as normalization) involves image pair radiometric matching, where any number of techniques can be employed to select pseudo-invariant features (PIFs) (Hall et al., 1991; Schott et al., 1988), which are subsequently used to empirically calibrate images in a time-series. Depending on the application, correction using image pairs need not include corrections for atmospheric and sensor related parameters and thus derivation of physical units such as reflectance. However, when physical surface units are desirable, it is essential that one image receives full absolute image correction, and then other images can be relatively normalized to it. This combined "absolute-normalization" approach may have certain advantages over the use of absolute procedures alone.

The main questions addressed in this paper include:

1) How do absolute (full and partial) and combined "absolute-normalization" correction methods compare when used to produce Landsat temporal reflectance trajectories for coniferous forest stands recovering from stand-replacing disturbance in western Oregon? We compare the partially corrected case (absolute calibration only) with several full correction methods (absolute calibration plus atmospheric correction) and (as suggested in Question 2) two "absolute-normalization" methods.
2) Are automated relative correction procedures based on statistical ordination as effective as those based on analyst-selected PIFs? The process of selecting PIFs, if done by the analyst, can be time consuming, particularly if more than two image dates are examined. Thus, an automated procedure could have great merit. The ordination procedure we use is called multivariate alteration detection (MAD).
3) How do absolute (partial and full) and "absolute-normalization" corrections affect the spectral manifestation of forest succession in remotely sensed imagery? As the ultimate purpose of a larger study is to characterize temporal spectral trajectories in relation to forest succession, it is important to determine how the different image correction methods compare in those terms.

2. Methods

2.1. Data and study area

The image dataset used in this study consists of 16 Landsat-5 TM and 3 Landsat-7 ETM+ images (WRS-2 path 46 row 29) from western Oregon ranging between 1984 and 2004 (Table 1). Only images acquired in summer months (July, August, and September) were considered. The available images were further screened based on the absence of cloud cover, however when

Table 1
Landsat time-series used in this study

Sensor	Date
TM	8/4/1984
TM	8/26/1986
TM	7/12/1987
TM	8/31/1988
TM	9/3/1989
TM	7/7/1991
TM	8/10/1992
TM	8/29/1993
TM	7/31/1994
TM	8/19/1995
TM	8/21/1996
TM	7/23/1997
TM	8/11/1998
TM	8/16/2000
TM	8/25/2003
TM	7/26/2004
ETM+	8/22/1999
ETM+	7/26/2001
ETM+	7/29/2002

multiple cloud free images were available for a given year, the image acquired closest to July 31 was selected for inclusion in the time-series. All images were resampled to a 30-m resolution and coregistered using an automated tie-point program (Kennedy & Cohen, 2003) to the 1987 image, which had been orthorectified by the United States Geological Survey. All images were coregistered to the UTM coordinate system (zone 10) with a root mean square error of less than 0.5 pixels per image.

The study area encompasses portions of three major ecological provinces including the Coastal Range (CR), Western Cascades (WC) and Willamette Valley (WV) (Franklin & Dyrness, 1988), as well as nearly the full elevation and climatic gradients present in western Oregon (Fig. 1). The area also includes a diverse distribution of existing land ownership categories (Cohen et al., 2002), therefore the image time-series represents the forest disturbance and recovery patterns present in response to the land use dynamics of the region.

2.2. Calibration and normalization

In this study we compared the effect of absolute correction (both full and partial, as described earlier) and combined "absolute-normalization" on temporal reflectance trajectories of

Fig. 1. Landsat 46/29 study area (adapted from Cohen et al., 2001).

recovering conifer forests. Radiometric correction was a multi-step process. For the final step, atmospheric correction, several different methods were used and compared.

2.2.1. Radiometric calibration

Radiometric Calibration was a multi-step process that involved the use of standard equations to convert 8-bit satellite-quantized calibrated digital numbers (DN) to at-satellite reflectance. Landsat-5 images were first converted to at-satellite radiance using Eq. (1),

$$L_{sat} = (DN - B)/G \tag{1}$$

where L_{sat} is band specific at-satellite radiance (W m^{-2} sr^{-1} µm^{-1}), DN is satellite quantized calibrated digital number, B is band specific bias in DN, and G is band-specific gain (m^2 sr µm W^{-1}). The impact of sensor degradation on the gain parameter was accounted for using data published by Thome et al. (1997) and Teillet et al. (2001), while revised gain parameters published by Chander and Markham (2003) were used for images acquired and processed after May 5, 2003. The biases reported by Markham and Barker (1986) were used for all images.

Landsat-7 images were converted to at-satellite radiance using Eq. (2),

$$L_{sat} = \left((LMAX_{sat} - LMIN_{sat})/(DNMAX - DNMIN) \right) \times (DN - DNMIN) + LMIN_{sat} \tag{2}$$

where $LMAX_{sat}$ is band-specific spectral radiance scaled to DNMAX (W m^{-2} sr^{-1} µm^{-1}), $LMIN_{sat}$ is band-specific spectral radiance scaled to DNMIN (W m^{-2} sr^{-1} µm^{-1}), DNMAX is maximum quantized calibrated digital number (255), and DNMIN is minimum-quantized calibrated digital number (0 for LPGS data, 1 for NLAPS data). Eq. (2) accounts for gain state (i.e., high/low setting) by using the respective published LMIN/LMAX values (Landsat-7 Science Data Users Handbook).

After conversion to at-satellite radiance, each image was converted to at-satellite reflectance (assuming a uniform Lambertian surface under cloudless conditions) using Eq. (3),

$$\rho_{ASR} = \frac{(\pi * L_{sat})}{(E_0 * \cos(\Theta))} \tag{3}$$

where ρ_{ASR} is at-satellite reflectance, E_0 is exoatmospheric solar constant (W m^{-2} µm^{-1}) (corrected for solar distance), and Θ is solar zenith angle. By definition, at-satellite reflectance does not remove atmospheric effects, thus it is referred to here as the partially corrected case.

2.2.2. Atmospheric correction

For full absolute correction, at-satellite reflectance was converted to surface reflectance (assuming a uniform Lambertian surface under cloudless conditions) using Eq. (4),

$$\rho = \frac{\pi(L_{sat} - L_p)}{T_v(E_0 * \cos(\Theta) * T_z + E_{down})} \tag{4}$$
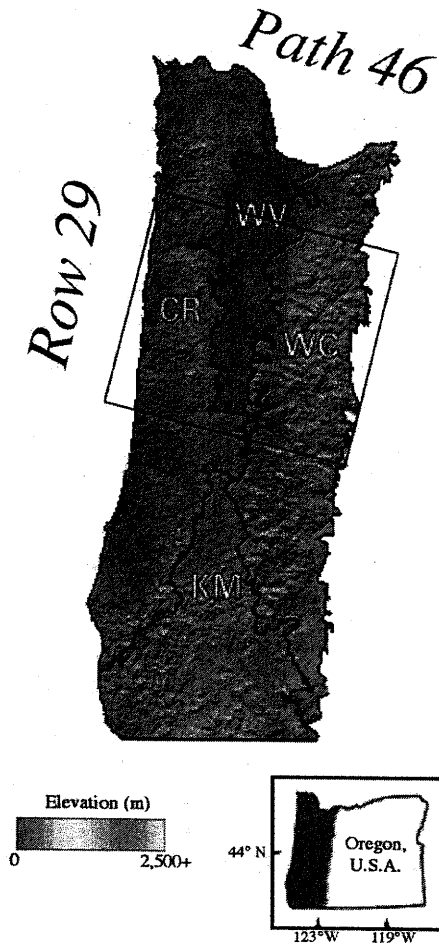
where ρ is estimated surface reflectance, L_p is path radiance (W m^{-2} sr^{-1} μm^{-1}), T_v is atmospheric transmittance from the target toward the sensor, T_z is atmospheric transmittance in the illumination direction, and E_{down} is downwelling diffuse irradiance (W m^{-2} μm^{-1}). To derive values of the atmospheric correction coefficients T_z, T_v, E_{down} and L_p in Eq. (4) we use three different atmospheric correction methods. These methods included dark object subtraction (DOS), modified dense dark vegetation (MDDV), and second simulation of the satellite signal in the solar spectrum (6 s). These methods range in complexity from a simple image-based correction procedure (DOS) to a detailed, theoretical model based on radiative transfer theory (6 s).

2.2.2.1. Dark Object Subtraction (DOS).

The DOS method assumes that within a satellite image there exist features that have near-zero percent reflectance (i.e., water, dense forest, shadow), such that the signal recorded by the sensor from those features is solely a result of atmospheric scattering (path radiance), which must be removed (Chavez Jr., 1996). Path radiance, L_p, was estimated using Eq. (5),

$$L_p = G*DN_{dark} + B - 0.01[E_0 * \cos(\Theta) * T_z + E_{down}]T_v/\pi \quad (5)$$

where DN_{dark} is the darkest DN value in each spectral band with at least one thousand pixels (Teillet & Fedosejevs, 1995). The DOS method used here is referred to in Song et al. (2001) as DOS3, which estimates T_v as $e^{-\tau/\cos(\Theta_v)}$ and T_z as $e^{-\tau/\cos(\Theta_z)}$ assuming a Rayleigh atmosphere with no aerosols and one percent surface reflectance for the dark object. Optical thickness for Rayleigh scattering (τ_r) (Kaufman, 1989) was estimated by,

$$\tau_r = 0.008569 * \lambda^{-4}(1 + 0.0113 * \lambda^{-2} + 0.00013 * \lambda^{-4}) \quad (6)$$

where λ is the band-center wavelength in μm. E_{down} for a Rayleigh atmosphere was estimated as zero aerosol optical depth

at 550 nm using the 6 s radiative transfer code (Vermote et al., 1997). DOS3 was selected for use in this study in lieu of other DOS methods based on its ability to create a consistent common scale as evaluated by change detection and classification accuracy for part of the Landsat scene under investigation (Song et al., 2001).

2.2.2.2. Modified Dense Dark Vegetation (MDDV).

This approach is based on the dense dark vegetation (DDV) method (Liang et al., 1997), which assumes that areas of dense, dark vegetation are present in the satellite image in which to use as dark objects for Landsat bands 1 (blue) and 3 (red). Since longer spectral wavelengths are less affected by atmospheric scattering, Landsat band 7 at-satellite reflectance is assumed equal to its surface reflectance. As in Liang et al. (1997), dark areas were spatially defined for each image where band 7 reflectance was ≤ 0.05 and NDVI was >0.1. The identified dark areas were used to estimate band 1 and band 3 surface reflectance based on the following relationships with band 7 surface reflectance (Kaufman et al., 1997),

$$\rho_1 = \rho_7/4 \quad \rho_3 = \rho_7/2 \quad (7)$$

where the subscripts of ρ are Landsat band numbers. L_p for each image was estimated as the difference between the at-satellite reflectance in bands 1 and 3 and the estimated surface reflectance from Eq. (7). This approach was first used with a "smart moving window" (Liang et al., 1997) to atmospherically correct individual pixels, and was subsequently modified by Song et al. (2001) to a "fixed" window approach for band-wise correction as applied here. The presented MDDV approach derives an appropriate aerosol optical depth by iteratively running 6 s radiative transfer code until the output surface reflectance matches the predicted surface reflectance from Eq.
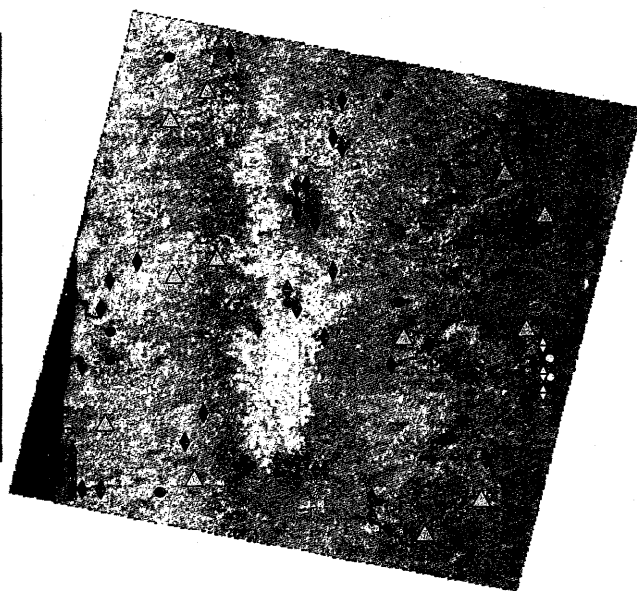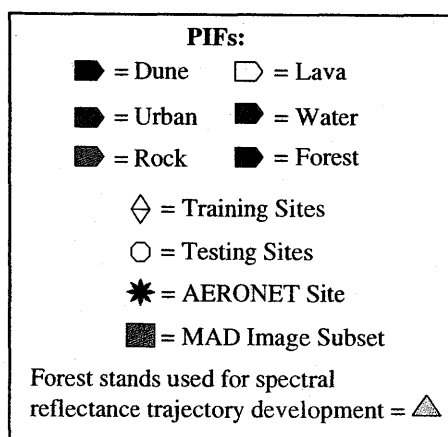
Fig. 2. Spatial location of hand-selected training and testing pseudo-invariant features (PIFs), multivariate alteration detection (MAD) image subset, forest stands used for spectral reflectance trajectory development and AERONET site in 46/29 Landsat scene.

(7). Matching aerosol optical depths were then used in 6 s to atmospherically correct the subsequent bands of each image.

2.2.2.3. Second simulation of the satellite signal in the solar spectrum (6 s).

The 6 s general radiative transfer code (Vermote et al., 1997) was used to estimate surface reflectance using aerosol optical depth (AOD) data collected at the AERONET site located at the HJ Andrews Experimental Forest in Blue River, Oregon (Fig. 2). Estimates of aerosol optical depth were acquired at 500 and 670 nm for the day and time closest to satellite overpass for the 1994 through 2004 images (except 2002, no data). The aerosol optical depth at 550 nm required as input to 6 s was derived for these images using Eq. (8),

$$\tau_\lambda = a * \lambda^b \tag{8}$$

where τ_λ is aerosol optical depth at wavelength λ (nanometers), and a and b are empirical parameters (Liang et al., 1997). The estimated aerosol optical depth at 550 nm (Table 2) was used along with the 6 s midlatitude summer atmosphere and continental aerosol model to derive surface reflectance for each image. As optical depth data were only available for 1994–2001 and 2003–2004, only images from these years could be corrected with 6 s.

2.2.3. Absolute-normalization

For "absolute-normalization", one atmospherically corrected image (1994) was chosen as the reference to which all others were adjusted, using two separate approaches: analyst selection of PIFs and statistical ordination (MAD) (Canty et al., 2004). This image was selected because of its high radiometric quality and its central location in the time-series. Because we used a fully (i.e., atmospherically) corrected reference image (6 s

version) for these procedures, we refer to them as two variants of an "absolute-normalization" approach.

2.2.3.1. Pseudo-invariant Feature (PIF).

Using the criteria for manually selecting normalization targets suggested by Eckhardt et al. (1990), the image time-series was thoroughly inspected to derive a total of 63 training PIFs (the same 33 dark and 30 bright features in each image) for relative normalization. The bright (dune, urban, rock) and dark (water, forest, lava) features were hand-selected to be well distributed around the image (Fig. 2), and to encompass the full range of spectral brightness values (bright, medium, dark) found. Normalization was accomplished on a band-by-band basis using these "training" PIFs with reduced major axis (RMA) regression (Canty et al., 2004; Cohen et al., 2003). An independent set of test PIFs (13 dark, 13 bright; $n=26$) was also manually selected (Fig. 2) for the purpose of validating the common scale produced by the absolute (both full and partial) and "absolute-normalization" correction methods.

2.2.3.2. Multivariate Alteration Detection (MAD).

Selecting PIFs by hand, as previously described, is a time-consuming task, particularly when the time-series consists of several images. An attractive and less subjective alternative for selecting PIFs is to use statistical methods to locate them automatically (Hall et al., 1991). One such method, multivariate alteration detection (MAD) (Canty et al., 2004; Nielsen et al., 1998) uses traditional canonical correlation analysis (CCA) (Hotelling, 1936) to find linear combinations between two groups of variables (i.e., the spectral bands of subject and reference images) ordered by correlation, or similarity between pairs. Differences between such ordered pairs are called MAD variates and these are invariant to affine transformations (including linear scaling). This implies that linear atmospheric and instrumental effects will not influence the change/no-change probabilities of the pixels derived from the method. In fact, the sum of squares of the standardized MAD components (the MAD components divided by their standard deviations) is approximately chi-square distributed, enabling no-change thresholds to be set easily. The MAD transformation was used here to locate invariant pixels (chi-square threshold 0.99) between each image in the time-series and the 1994 6 s corrected reference. The selected invariant pixels were subsequently used to normalize each image band-by-band to the reference scene using RMA regression.

2.3. Error analysis

The absolute (full and partial) and relative ("absolute-normalization") correction methods tested here all use linear adjustments to convert raw image DNs to units of estimated surface reflectance (or at-satellite reflectance in the partial correction case). Thus, each image in the time-series (except 6 s, applied only to images with available in situ atmospheric data) was converted to estimated surface reflectance using the look up table (LUT) approach described by Song et al. (2001).

After applying atmospheric corrections to the image time-series, a 3×3 window was placed over each test PIF (26 in number) and the mean spectral reflectance value for each band of

Table 2
Aerosol optical depth (AOD) at 550 nm estimated from HJ Andrews Aeronet site and the modified dense dark vegetation (MDDV) absolute correction method

Image	MDDV	AERONET
	AOD	AOD
1984	0.240	–
1986	0.230	–
1987	0.380	–
1988	0.370	–
1989	0.110	–
1991	0.400	–
1992	0.140	–
1993	0.090	–
1994	0.150	0.015
1995	0.290	0.010
1996	0.400	0.036
1997	0.110	0.028
1998	0.100	0.008
1999	0.110	0.032
2000	0.130	0.048
2001	0.090	0.029
2002	0.090	–
2003	0.130	0.093
2004	0.070	0.030

corrected imagery (5 methods × 18 images × 6 spectral bands + 9 6 s corrected images × 6 spectral bands = 594 band images in all) was extracted and compared to the mean PIF spectral reflectance values of the appropriate reference image. The difference between corrected PIF reflectance and the reference PIF reflectance is reported as the root mean square error (RMSE). Thus, all relatively normalized images were compared to the 6 s corrected 1994 reference image, whereas the absolutely corrected images were compared to the 1994 reference image corrected with its corresponding correction method (e.g., DOS3 corrected images were compared to the DOS3 1994 reference image; 6 s corrected images were compared to the 6 s corrected reference image, etc...). To assess robustness of correcting an image time-series, RMSE was calculated by image date (across spectral bands), by Landsat band (across image dates), and overall by correction method (across image dates and spectral bands). A typical RMSE for detailed absolute correction of Landsat imagery has been previously reported at 0.02 (Moran et al., 1992), therefore 0.02 will serve here as a benchmark for establishing successful image correction.

2.4. Spectral reflectance trajectories

The development of meaningful spectral reflectance trajectories is not solely dependent on the accurate calculation of true surface reflectance, but more on a consistent measurement of surface reflectance among images, which has previously been referred to as "common scale" (Song et al., 2001). The consistency of common scale is based here on the difference in spectral response among the corrected images, relative to its respective reference image over the set of test PIFs. The absolute (full or partial) or relative ("absolute-normalization") correction method found to have the least amount of spectral difference (lowest RMSE) among test PIFs will be used to derive the spectral reflectance trajectories of recovering conifer forests. If two methods have similarly low RMSEs, the method best lending itself to operational use will be selected for spectral trajectory development.

Forest stands undergoing stand-replacing disturbance between 1986 and 1987 were visually identified using a multi-temporal RGB color composite of spectral band 5. To evaluate the effect of image correction on the spectral manifestation of forest
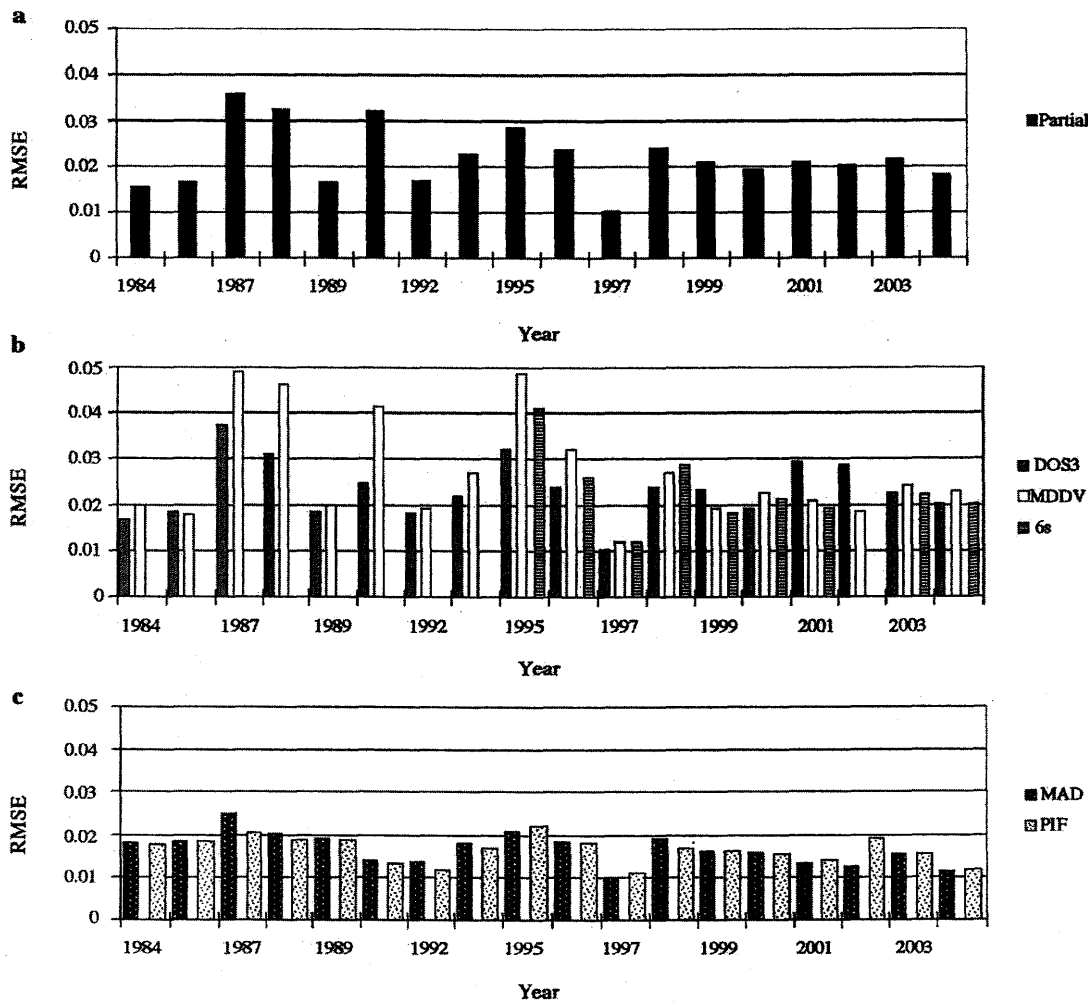
Fig. 3. RMSE by image (calculated across spectral bands) for (a) partial correction (absolute calibration only), (b) absolute corrections (absolute calibration plus atmospheric correction) and (c) relative corrections (absolute correction plus image normalization).
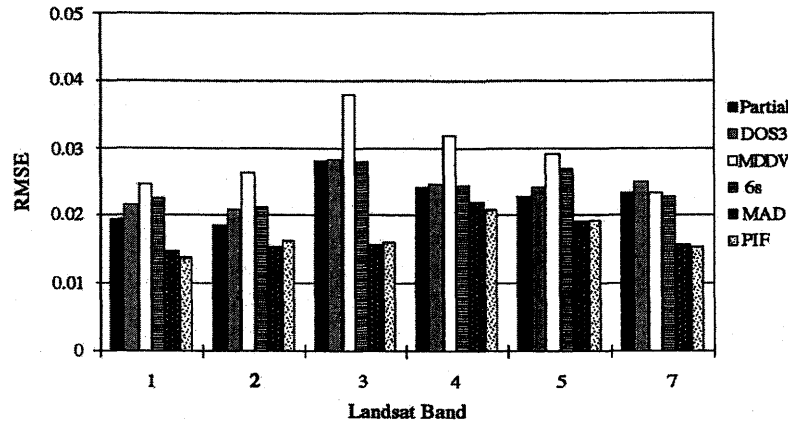
Fig. 4. RMSE by Landsat band (across image dates) for all image correction methods.

succession, twelve forest stands were hand-selected for spectral reflectance trajectory development. Of the twelve forest stands selected (Fig. 2), six were located in the Coast Range (CR) and six in the Western Cascades (WC) ecological provinces. Stand mean reflectance values were extracted from the time-series corrected with the preferred image correction method, as well as from the partially corrected (absolute calibration only) image time-series and fit with quadratic polynomial curves. These quadratic polynomial curves, or spectral reflectance trajectories were developed for all six Landsat spectral bands, as well as for the tasseled cap transformation (brightness, greenness, wetness) and the normalized difference vegetation index (NDVI). Standard error (RMSE) and variance explained (R^2) were calculated for each quadratic polynomial model, then averaged across the twelve forest stands to determine whether the trajectory models were improved (i.e., lower RMSE) by image correction.

3. Results

3.1. Image correction

3.1.1. RMSE by image date

To evaluate the consistency of common scale at the image level, RMSE was calculated for each image date (across spectral bands) by image correction method (Fig. 3). Examining RMSE for the partially corrected images (Fig. 3a) reveals the surprisingly consistent spectral response of the image time-series even with no atmospheric corrections applied. The consistent nature of the partially corrected time-series is expressed by seven of the eighteen images (1984, 1986, 1989, 1992, 1997, 2000 and 2004) having less than 0.02 RMSE, with seven others (1993, 1996, 1998, 1999, 2001, 2002, and 2003) falling just slightly above the 0.02 benchmark. Only four images (1987, 1988, 1991, and 1995) were considered appreciably different than the reference image, with RMSEs nearly equal to or greater than 0.03.

Only nine of the eighteen images in the time-series were corrected using all three full absolute correction methods (Fig. 3b), thus reducing the number of observations to assess improvements to the common scale of the full time-series. Of these nine images, DOS3 had the lowest RMSE in six of the images, compared to three for 6 s. The MDDV method yielded

the highest RMSE of all the absolute correction methods in six of these nine images. In order to determine whether the common scale was improved by full absolute correction, the partially corrected image time-series was used as a standard for comparison. Of the nine images that were corrected by all three absolute methods, only four (1998, 1999, 2000, and 2001) had lower RMSEs than their partially corrected counterparts. Of the four images with improved common scale resulting from absolute correction, two were corrected with DOS3 and two with 6 s. Thus, the least complex DOS3 method proved to be the most effective absolute correction method. It yielded the lowest RMSE in six of the nine images corrected with all three absolute methods, and slightly lowered RMSE from that which was observed in the partially corrected images. Even so, the common scale of the image time-series was not consistently improved by any of the full absolute correction methods.

On the other hand, the image time-series relatively normalized with the two "absolute-normalization" methods appears consistently improved in terms of common scale (Fig. 3c). All eighteen images had at least one relative method yield an RMSE of 0.02 or less. Compared to the partially corrected time-series, fifteen of the images had lower RMSEs after relative normalization. Overall, it appears that the improved common scale was achieved nearly equally by both the PIF and MAD methods. Though differences in RMSE were slight between the two methods, PIF did have lower RMSEs for eleven of the eighteen images in the full time-series.
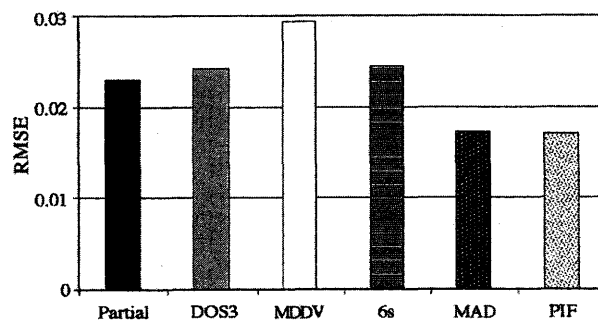
Fig. 5. RMSE by image correction method (across all image dates and spectral bands).

3.1.2. RMSE by Landsat band

The consistency of the image time-series was also evaluated based on RMSE by Landsat band (across images) (Fig. 4). Shorter wavelength spectral bands like Landsat bands 1 and 2 are commonly impacted by Rayleigh scattering. Although scattering is likely, bands 1 and 2 do not seem significantly impacted here as both have low (<0.02) partially corrected RMSEs. On the other hand, band 3 has the highest partially corrected RMSE, which may be attributed to atmospheric scattering. Longer spectral regions like Landsat bands 4, 5 and 7 are typically influenced by atmospheric absorption, which is likely contributing to the elevated (>0.02) partially corrected RMSEs observed for these spectral bands.

If the errors detailed above are truly a result of atmospheric scattering and absorption, then it stands to reason that full absolute correction would likely account for some of these effects, serving to lower RMSE from that observed in the partially corrected images. Quite the opposite is observed however, with all of the absolute methods yielding an increase in RMSE in four (1, 2, 4, and 5) of the six spectral bands. In fact, all of the absolute methods failed to lower RMSE to <0.02. DOS3 and 6 s yielded similar RMSEs in four (1–4) of the six spectral bands; two (3 and 4) of which were nearly equal to the error observed in partial correction. On the other hand, MDDV yielded the highest RMSEs of all the methods tested in five (1, 2, 3, 4, and 5) of the six spectral bands. Overall, full absolute correction did not improve the consistency of common scale from that observed in the partially corrected images.

Relative "absolute-normalization" on the other hand significantly improved the image time-series from the spectral perspective. Both of the relative correction methods lowered RMSE from that observed in partial correction. In fact, after

relative normalization five of six spectral bands had at least one relative method lower RMSE to <0.02. In terms of lowering RMSE from partial correction, band 4 seemed least improved by relative normalization whereas band 3 the most. Both of the relative "absolute-normalization" methods performed nearly equally in all six spectral bands.

3.1.3. RMSE by image correction method

To assess overall effectiveness RMSE was calculated for each image correction method (across all images and spectral bands) (Fig. 5). Similar to observations by image and by Landsat band, none of the full absolute correction methods reduced the RMSE below that observed in the partially corrected data. The MDDV method produced the greatest overall error, with the DOS3 and 6 s methods resulting in slight increases in the error observed in the partially corrected images. The relative "absolute-normalization" methods were equally effective, reducing the error observed in the partially corrected images by nearly 25%. The PIF method produced a slightly lower overall RMSE than MAD.

3.2. Spectral reflectance trajectories

Although the PIF method yielded slightly less error than MAD, there was very little difference between the two relative "absolute-normalization" methods in terms of improving the common scale of the image time-series. Given the similarity of the two methods, the MAD "absolute-normalization" approach is preferred here for several reasons (see Discussion) including its utility to operational use. As a result, spectral reflectance trajectories were developed using the MAD "absolute-normalization" and the partially corrected image time-series. The parameters (R^2 and RMSE) of the quadratic polynomial models used to form the spectral reflectance trajectories were averaged across the twelve hand-selected forest stands and are presented in Table 3.

The results indicate that on average, the MAD "absolute-normalization" spectral reflectance trajectories have less residual scatter (i.e., lower mean RMSE across stands) than trajectories created with the partially corrected time-series. Although MAD band 1 and 2 trajectories yield the lowest post-correction errors, they explain a relatively low percentage of variance as expressed by R^2. On the other hand, NDVI spectral reflectance trajectories explain a high percentage of variation found in the temporal data, yet yield high prediction errors. Ideally, models capturing a high percentage of variation combined with low prediction error would produce the best spectral reflectance trajectories. In this regard, trajectories created with MAD "absolute-normalization" band 7 and tasseled cap wetness seem promising for characterizing the dynamic process of forest succession.

4. Discussion

4.1. Atmospheric correction versus "absolute-normalization"

The results indicate that the full absolute correction methods tested here were ineffective at correcting satellite images to a consistent common scale, a finding similarly reported by Song et al. (2001) for a portion of the same Landsat scene. The more

Table 3
R-square and RMSE of quadratic polynomial models averaged across twelve forest stands recovering from stand-replacing disturbance for partial and MAD "absolute-normalization" image correction methods

		R^2 Mean	RMSE Mean
Band 1	Partial	0.62	0.0107
	MAD	0.51	0.0057
Band 2	Partial	0.63	0.0088
	MAD	0.56	0.0054
Band 3	Partial	0.77	0.0141
	MAD	0.72	0.0105
Band 4	Partial	0.54	0.0379
	MAD	0.84	0.0255
Band 5	Partial	0.82	0.0217
	MAD	0.77	0.0208
Band 7	Partial	0.90	0.0124
	MAD	0.91	0.0109
Brightness	Partial	0.36	0.0390
	MAD	0.31	0.0254
Greenness	Partial	0.84	0.0226
	MAD	0.91	0.0181
Wetness	Partial	0.92	0.0138
	MAD	0.93	0.0133
NDVI	Partial	0.92	0.0426
	MAD	0.90	0.0410

complex methods (MDDV and 6 s) attempt to estimate aerosol optical depth, which generally rely on various simplifying assumptions. These assumptions have been previously reported as ineffective for improving change detection and classification accuracies (Song et al., 2001) and have not served to improve the common scale of the image time-series presented here. Given the relatively stable common scale observed in the partially corrected data, it is not surprising that complex theoretical adjustments reduced the spectral consistency of the image time-series. While simple corrections like DOS3 generally worked the best, none of the full absolute correction methods produced a common scale more consistent than observed in the partially corrected images.

The MDDV method was the least effective absolute correction method, and as reported in other studies, tends to significantly over-estimate aerosol optical depth (Table 2). This over-estimation resulted in a disproportionate amount of dark features (water and mature forest) being converted to near zero values in bands 1 and 3, yielding over-corrected water and forest spectral signatures. Based on observations in this study it is likely that the criteria for defining dark areas (band 7 reflectance ≤ 0.05 and NDVI > 0.1) is too liberal. More stringent criteria for defining dark areas may improve the performance of this method, especially for highly vegetated Landsat scenes. Furthermore, the partially corrected data also suggests that band 7 may be impacted by atmospheric absorption, perhaps invalidating the MDDV assumption that band 7 at-satellite reflectance equals band 7 surface reflectance.

Although the most complex method, 6 s was slightly less effective than the much simpler DOS3 method at creating a consistent common scale. The AOD data used in 6 s were collected at the Western Cascade AERONET site, located at the HJ Andrews Experimental Forest. Since Landsat scene 46/29 lies adjacent to the Pacific Ocean and covers portions of two mountain ranges it is likely, given the highly variable nature of aerosol loadings, that AOD estimates recorded in the Western Cascades may differ significantly from those observed elsewhere in the scene. Since accurate AOD data is often difficult to obtain, improving image-based estimates from methods like MDDV warrant further investigation. Determining the success of 6 s as an absolute correction method was further limited by the lack of AOD data for the full temporal span of the image time-series.

Whether analyzed by image date, by Landsat band, or overall by image correction method, relative normalization applied in the "absolute-normalization" context produced the most consistent common scale for the image time-series. This finding is similar to Olsson (1995), who reported that relative normalization was to be preferred to absolute correction for accurate detection of localized changes in boreal forests. Although the PIF method had a slightly lower overall RMSE, there are several reasons for preferring MAD.

First, MAD is easier and more time efficient to implement than PIF. Although hand-selecting invariant features has been successfully employed in other studies, it is a time consuming process that is often subject to analyst interpretation, and potentially limited by scene location. The MAD method however, has been automated to statistically locate invariant pixels in a small subset (Fig. 2) taken from the subject and reference images. Tests

(not presented) show that the performance of normalization can vary depending on the quality and quantity of invariant pixels selected from subsets taken from different areas of the full Landsat scene. Selecting a subset that contains large, highly stable (i.e., low variance) bright features like sand dunes and stable dark features like water and mature forest should be preferred. Although mature forest is likely to change spectrally from year to year due to phenological differences, it seems capturing this natural variability in the normalization model will facilitate separation of real forest change from noise. A simple test can be conducted to locate several suitable image subsets per Landsat scene for future implementation of MAD. In addition, the MAD program is currently being modified to integrate invariant pixels selected from multiple image subsets into one normalization model.

The second advantage to using MAD is that areas of significant change (i.e., disturbance, cloud cover) occurring between the subject and reference images do not need to be accounted for prior to selecting invariant pixels. Other methods for statistically selecting invariant pixels, such as ordination by principal components analysis (PCA) have been previously suggested (Du et al., 2002). While this method has produced favorable results, it typically requires more processing time as PCA is not invariant to linear scaling of input data. Hence, significant areas of change between the subject and reference image (i.e., clouds) must be masked out prior to statistical ordination. PCA can also be significantly weighted by a single image in the time-series that has high variance. Since the basis for MAD is CCA, pixels that significantly change between the subject and reference image do not need to be masked prior to ordination, offering additional time savings when correcting multiple images.

Although atmospheric correction is not required before running MAD, it may be useful to have all the images in the time-series normalized to units of surface reflectance. Thus, the third advantage to using MAD is that since it is invariant to linear scaling, all images in a time-series can be corrected for atmospheric effects while simultaneously being converted to units of reflectance. This is best achieved by using the "absolute-normalization" approach suggested here, where the selected reference scene is first converted to surface reflectance using one of the full absolute correction methods, and then all other images are normalized to it. It is important to note that linear transformations such as sensor gain/bias adjustments and atmospheric corrections are not necessary prior to running MAD. The same consistency of common scale will be achieved with MAD with or without corrections to the reference image, offering additional savings in processing time depending on user needs.

4.2. Spectral reflectance trajectories

The objective of radiometric correction is not primarily to improve the percentage of variance explained (R^2) by a spectral reflectance trajectory, but rather to reduce the noise associated with multi-date data, thus lowering residual scatter (RMSE). Our results indicate that for all spectral bands and indices evaluated, that "absolute-normalization" using MAD produced spectral

reflectance trajectories with less residual scatter than trajectories created with the partially corrected images. Although normalization effectively reduced residual scatter, two factors contributed to a less than expected magnitude of improvement. First, images acquired in western Oregon during the summer months already have a high degree of spectral consistency due to seasonally dry conditions. Second, image correction error is evaluated here by comparing atmospherically corrected images to images subjected to partial correction (e.g., sun and view angle effects), likely reducing the magnitude of improvement derived from a comparison against uncorrected images (e.g., DN). We are currently using MAD to normalize images acquired in more spectrally diverse forest types (i.e., eastern deciduous) to assess the level of improvement "absolute-normalization" can make to those types of spectral reflectance trajectories.

Now that we have determined that "absolute-normalization" using MAD effectively improves the development of spectral reflectance trajectories, our focus turns to using the normalized spectral reflectance trajectories to analyze spatial patterns of forest succession. Our observations indicate that spectral reflectance trajectories developed with MAD normalized band 7 and tasseled cap wetness seem promising for characterizing continuous attributes of forest succession. It should be noted however, that spectral reflectance trajectories are built here on single variables, while models of successional recovery after disturbance will likely include multiple variables.

5. Conclusion

An effective and efficient method for atmospherically correcting an image time-series for characterization of forest successional patterns, referred to as "absolute-normalization", was presented. This method relatively normalizes all images in a time-series to an atmospherically corrected reference image. The benefits of this approach are the reliance on the more dependable relative normalization process to yield an improved temporal common scale, while subsequently converting all images in a time-series to units of surface reflectance. The results demonstrated how converting images in a time-series to reflectance using absolute correction alone tends to decrease the consistency of common scale compared to that observed in partially corrected images.

Overall, the MDDV method was the least effective absolute method, possibly resulting from the overly lenient spatial definition of dark areas. Although the most complex method, the 6 s radiative transfer code performed slightly worse than the much simpler DOS3 method, with possible shortcomings attributed to the extrapolation of point sampled AOD data to the full Landsat scene. The image based DOS3 method did the best job of all the absolute methods at correcting the image time-series, supporting the assertion that simpler atmospheric correction methods may be preferred when consistency of common scale is more important than accurate estimation of surface reflectance (Song et al., 2001).

The best normalization results, in terms of RMSE, were achieved nearly equally by both relative "absolute-normalization" methods, with correction based on analyst selected PIFs generating only a slightly more accurate common scale than relative correction based on invariant pixels statistically selected by the MAD algorithm. Although the PIF method generated slightly lower overall errors, several reasons emerged for preferring the MAD based approach to invariant feature selection. These reasons include ease and time efficiency of implementation and invariance to linear scaling effects. The "absolute-normalization" approach using MAD as presented here is also preferred for the simultaneous correction of atmospheric effects during the relative conversion to surface reflectance. While previously shown to work well in arid environments (Canty et al., 2004), the MAD algorithm has been shown here to generate a temporally consistent, spectrally diverse range of invariant pixels for successful normalization of a highly forested Landsat time-series.

To assess the impact of image normalization on the characterization of recovering conifer forests, spectral reflectance trajectories were developed for twelve hand-selected forest stands undergoing stand-replacing disturbance. For all spectral bands and indices evaluated, MAD normalized spectral reflectance trajectories had less residual scatter (lower RMSE) than trajectories created with the partially corrected images.

References

Canty, M. J., Nielsen, A. A., & Schmidt, M. (2004). Automatic radiometric normalization of multitemporal satellite imagery. *Remote Sensing of Environment, 91*(3–4), 441–451.

Chander, G., & Markham, B. (2003). Revised Landsat-5 TM radiometric calibration procedures and postcalibration dynamic ranges. *IEEE Transactions on Geoscience and Remote Sensing, 41*(11), 2674–2677.

Chavez Jr., P. S. (1996). Image-based atmospheric correction — Revisited and improved. *Photogrammetric Engineering and Remote Sensing, 62*(9), 1025–1036.

Cohen, W. B., Fiorella, M., Gray, J., Helmer, E., & Anderson, K. (1998). An efficient and accurate method for mapping forest clearcuts in the Pacific Northwest using Landsat imagery. *Photogrammetric Engineering and Remote Sensing, 64*, 293–300.

Cohen, W. B., & Goward, S. N. (2004). Landsat's role in ecological applications of remote sensing. *Bioscience, 54*(6), 535–545.

Cohen, W. B., Maiersperger, T. K., Gower, S. T., & Turner, D. P. (2003). An improved strategy for regression of biophysical variables and Landsat ETM+ data. *Remote Sensing of Environment, 84*, 561–571.

Cohen, W. B., Maiersperger, T. K., Spies, T. A., & Oetter, D. R. (2001). Modelling forest cover attributes as continuous variables in a regional context with Thematic Mapper data. *International Journal of Remote Sensing, 22*(12), 2279–2310.

Cohen, W. B., Spies, T. A., Alig, R. J., Oetter, D. R., Maiersperger, T. K., & Fiorella, M. (2002). Characterizing 23 years (1972–95) of stand replacement disturbance in western Oregon forests with Landsat imagery. *Ecosystems, 5*, 122–137.

Cohen, W. B., Spies, T. A., & Fiorella, M. (1995). Estimating the age and structure of forests in a multi-ownership landscape of western Oregon, U.S.A. *International Journal of Remote Sensing, 16*(4), 721–746.

Du, Y., Teillet, P. M., & Cihlar, J. (2002). Radiometric normalization of multitemporal high-resolution satellite images with quality control for land cover change detection. *Remote Sensing of Environment, 82*, 123–134.

Eckhardt, D. W., Verdin, J. P., & Lyford, G. R. (1990). Automated update of an irrigated lands GIS using SPOT HRV imagery. *Photogrammetric Engineering and Remote Sensing, 56*(11), 1515–1522.

Fiorella, M., & Ripple, W. J. (1993). Analysis of conifer forest regeneration using Landsat Thematic Mapper data. *Photogrammetric Engineering and Remote Sensing, 59*(9), 1383–1388.

Foody, G. M., Palubinskas, G., Lucas, R. M., Curran, P. J., & Honzak, M. (1996). Identifying terrestrial carbon sinks: Classification of successional stages in regenerating tropical forest from Landsat TM data. *Remote Sensing of Environment, 55*, 205–216.

Franklin, J., & Dyrness, C. (1988). *Natural vegetation of Oregon and Washington.* Corvallis, OR: Oregon State University Press.

Franklin, S. E., Moskal, L. M., Lavigne, M. B., & Pugh, K. (2000). Interpretation and classification of partially harvested forest stands in the Fundy Model forest using multitemporal Landsat TM digital data. *Canadian Journal of Remote Sensing, 26*(4), 318–333.

Hall, F. G., Botkin, D. B., Strebel, D. E., Woods, K. D., & Goetz, S. J. (1991). Large-scale patterns of forest succession as determined by remote sensing. *Ecology, 72*(2), 628–640.

Healey, S., Zhiqiang, Y., Cohen, W. B., & Pierce, D. J. (2006). Application of two regression-based methods to estimate the effects of partial harvest on forest structure using Landsat data. *Remote Sensing of Environment, 101*, 115–126.

Horler, D. N. H., & Ahern, F. J. (1986). Forestry information content of Thematic Mapper data. *International Journal of Remote Sensing, 7*(3), 405–428.

Hotelling, H. (1936). Relations between two sets of variates. *Biometrika, XXVIII*, 321–377.

Jakubauskas, M. E. (1996). Thematic Mapper characterization of lodgepole pine seral stages in Yellowstone National Park, USA. *Remote Sensing of Environment, 56*, 118–132.

Kaufman, Y. J. (1989). The atmospheric effect on remote sensing and its correction. In G. Asrar (Ed.), *Theory and Application of Optical Remote Sensing.* New York. 314ff.

Kaufman, Y. J., Wald, A., Remer, L. A., Gao, B., Li, R., & Flynn, L. (1997). The MODIS 2.1 μm channel — Correlation with visible reflectance for use in remote sensing of aerosol. *IEEE Transactions on Geoscience and Remote Sensing, 35*, 1–13.

Kennedy, R. E., & Cohen, W. B. (2003). Automated designation of tie-points for image-to-image coregistration. *International Journal of Remote Sensing, 24* (17), 3467–3490.

Liang, S., Fallah-Adl, H., Kalluri, S., JaJa, J., Kaufman, Y. J., & Townshend, J. R. G. (1997). An operational atmospheric correction algorithm for Landsat Thematic Mapper imagery over the land. *Journal of Geophysical Research, 102*, 17,173–17,186.

Markham, B. L., & Barker, J. L. (1986). Landsat MSS and TM post-calibration dynamic ranges, exoatmospheric reflectance and at-satellite temperature. *EOSAT Landsat Technical Notes, 1*, 3–8.

Mausel, P., Wu, Y., Yinghong, L., Moran, E. F., & Brondizio, E. S. (1993). Spectral identification of successional stages following deforestation in the Amazon. *Geocarto International, 4*, 61–71.

Miller, J. D., & Yool, S. R. (2002). Mapping forest post-fire canopy consumption in several overstory types using multi-temporal Landsat TM and ETM data. *Remote Sensing of Environment, 82*, 481–496.

Moran, M. S., Jackson, R. D., Slater, P. N., & Teillet, P. M. (1992). Evaluation of simplified procedures for retrieval of land surface reflectance factors from satellite sensor output. *Remote Sensing of Environment, 41*, 169–184.

Nielsen, A. A., Conradsen, K., & Simpson, J. J. (1998). Multivariate alteration detection (MAD) and MAF post-processing in multispectral, bitemporal image data: New approaches to change detection studies. *Remote Sensing of Environment, 64*, 1–19.

Nilson, T., Olsson, H., Anniste, J., Lukk, T., & Praks, J. (2001). Thinning-caused change in reflectance of ground vegetation in boreal forests. *International Journal of Remote Sensing, 22*(14), 2763–2776.

Olsson, H. (1995). Reflectance calibration of Thematic Mapper data for forest change detection. *International Journal of Remote Sensing, 16*(1), 81–96.

Peterson, U., & Nilson, T. (1993). Successional reflectance trajectories in northern temperate forests. *International Journal of Remote Sensing, 14*(3), 609–613.

Sabol, D. E., Gillespie, A. R., Adams, J. B., Smith, M. O., & Tucker, C. J. (2002). Structural stage in Pacific Northwest forests estimated using simple mixing models of multispectral images. *Remote Sensing of Environment, 80*, 1–16.

Sader, S. A., Bertrand, M., & Wilson, E. H. (2003). Satellite change detection of forest harvest patterns on an industrial forest landscape. *Forest Science, 49* (3), 341–353.

Schott, J. R., Salvaggio, C., & Volchok, W. J. (1988). Radiometric scene normalization using pseudoinvariant features. *Remote Sensing of Environment, 26*, 1–16.

Song, C., & Woodcock, C. E. (2003). Monitoring forest succession with multitemporal Landsat images: Factors of uncertainty. *IEEE Transactions on Geoscience and Remote Sensing, 41*(11), 2557–2567.

Song, C., Woodcock, C. E., Seto, K. C., Pax-Lenney, M., & Macomber, S. A. (2001). Classification and change detection using Landsat TM data: When and how to correct atmospheric effects. *Remote Sensing of Environment, 75*, 230–244.

Teillet, P. M., Barker, J. L., Markham, B. L., Irish, R. R., Fedosejevs, G., & Storey, J. C. (2001). Radiometric cross-calibration of the Landsat-7 ETM+ and Landsat-5 TM sensors based on tandem data sets. *Remote Sensing of Environment, 78*, 39–54.

Teillet, P. M., & Fedosejevs, G. (1995). On the dark target approach to atmospheric correction of remotely sensed data. *Canadian Journal of Remote Sensing, 21*, 375–381.

Thome, K., Markham, B., Barker, J., Slater, P., & Biggar, S. (1997). Radiometric calibration of Landsat. *Photogrammetric Engineering and Remote Sensing, 63*, 853–858.

van Wagtendonk, J. W., Root, R. R., & Key, C. H. (2004). Comparison of AVIRIS and Landsat ETM+ detection capabilities for burn severity. *Remote Sensing of Environment, 92*(3), 397–408.

Vermote, E. F., Tanre, D., Deuze, J. L., Herman, M., & Morcrette, J. J. (1997). Second simulation of the satellite signal in the solar spectrum, 6 S: An overview. *IEEE Transactions on Geoscience and Remote Sensing, 35*, 895–934.

Viedma, O., Meliá, J., Segarra, D., & García-Haro, J. (1997). Modeling rates of ecosystem recovery after fires by using Landsat TM data. *Remote Sensing of Environment, 61*, 383–398.